Available online at www.sciencedirect.com
ScienceDirect
Journal of Sound and Vibration 323 (2009) 257–269
JOURNAL OF SOUND AND VIBRATION
www.elsevier.com/locate/jsvi

Vibrations induced by harmonic loadings applied at circular rigid plate on half-space medium

Gin-Show Liou*

Department of Civil Engineering, National Chiao-Tung University, Hsin-Chu, Taiwan 30049

Received 26 June 2008; received in revised form 5 December 2008; accepted 21 December 2008
Handling Editor: L.G. Tham
Available online 11 February 2009

Abstract

The paper presents a systematic scheme to calculate the vibration at any specific location on a half-space medium due to harmonic vibrations of a circular rigid plate on the medium. In the scheme, the analytic solutions of 3D wave equations in cylindrical coordinates are employed. The vibration at any specific location on half-space medium is obtained analytically by a semi-infinite integration with respect to wave number k from 0 to ∞. Because of decaying nature of integrand with respect to wave number k, the numerical integration can only be performed up to a certain upper limit k_u instead of ∞ without loosing accuracy. The choosing of the integration upper limit k_u is dependent upon the factors of nondimensional vibration frequency and nondimensional distance between vibration source and receiving location. From the numerical results, one finds that some components of vibration on the surface may not attenuate monotonically along the distance from source. Some verification for the accuracy of the presented scheme will be made, and selected numerical results will be shown and discussed. Comments on the presented scheme will be given, and the presented scheme is proved to be effective and efficient for accurately predicting the vibrations on the surface induced by harmonic loadings applied at rigid circular plate.

1. Introduction

Environmental vibrations near vibration source will affect the performance of high precision equipments or hi-tech production machines; e.g. optical tools used by microelectronics industry. Therefore how to specify the allowance of ground vibration for those hi-tech production equipments and how to evaluate the ground vibration due to a specific vibration source have become important issues for design and construction of hi-tech production plants.

In response to the first problem, Gordon and Dresner [1] have proposed the generic vibration criterion curves for different vibration sensitive equipments. From these curves, one can find the allowable ground vibration is getting smaller as the production requirement is getting stricter. To address the second problem Sheng et al. [2] and Krylov [3] employed Euler beam theory to model whole track including rails, sleepers and ballast, and Kaynia et al. [4], Takemiya and Bian [5,6] proposed a more sophisticate analysis model, which

*Tel.: +886 3 5131469; fax: +886 3 5716257.
E-mail address: gsliou@mail.nctu.edu.tw

0022-460X/$ - see front matter © 2009 Elsevier Ltd. All rights reserved.
doi:10.1016/j.jsv.2008.12.025

takes dynamic interaction into account, to evaluate the ground vibration induced by passing train. To reduce the ground vibrations near track, open or in-fill trenches are usually recommended. Ahmad and Al-Hussaini [7] and Dasgupta et al. [8] have done some theoretical studies. Moreover, if the track is elevated on bridges, the ground vibration due to the excitations by bridge abutments will produce more serious problem to the hi-tech production tools. Takemiya [9] designed a wave impeding barrier of honeycomb piles to reduce the ground vibrations near bridge abutments. Therefore, the evaluation of ground vibrations induced by vibration of bridge foundation due to highway traffic or passage of train is very important for high precision production equipments nearby.

Most above mentioned analysis models, finite element or boundary element based methods are employed to model half-space medium or layered half-space medium. Regarding the analytical approach to evaluate the ground vibration due to specific sources, Miller and Pursey [10] have calculated the energy flux of compressional, shear and Rayleigh waves in the far-field of a semi-infinite medium generated by vertical harmonic vibration of circular plate, and Apsel and Ruco [11] have calculated the vibration in half-space medium due to point source (Green's Function). Also, from the practical point of view, Woods and Jedele [12] collected some observation data and deduced these data into a simple formula expressing the attenuation relationship of vibration in terms of distance and soil damping.

The paper will employ an semi-analytic scheme to calculate the vibration at any location on half-space medium due to harmonic vibration of a rigid circular plate. The term "semi-analytic" used to describe the scheme is because the semi-infinite integration of analytic solution will be replaced with a finite integration. The components of harmonic vibration of the plate are torsional, vertical, horizontal and rocking motions. In the scheme, the technique, developed by Liou [13], to decompose the applied tractions induced by vibrations of plate has been employed to solve the problem of wave propagation in half-space medium. These decomposed tractions will be easily fitted into the analytic solutions of 3D wave equations in cylindrical coordinates. This technique has been employed to generate the impedance functions for circular plate on half-space medium by Liou et al. [14]. The presented scheme in the paper will extend the work of Liou et al. [14] to generate the vibration at any location on half-space medium due to a harmonic loading applied at a rigid circular plate.

The formulation of the presented scheme can be derived from the work by Liou et al. [14] and the expression for the vibration at a specific location on half-space medium will end up with a semi-infinite integration with respect to wave number k. However, from the decaying nature of the integrand with respect to k, the vibration can be calculated by integration only up to a certain upper limit k_u without losing accuracy.

Some selected numerical results for a rigid circular plate subjected to torsional, vertical, and horizontal loadings are presented to demonstrate the effectiveness and efficiency of the proposed scheme .The numerical results will be verified by a special case and presented in nondimensional forms. In the numerical investigations, some numerical aspects regarding integration scheme, selection of k_u and influence of nondimensional frequency and distance on the numerical scheme will be discussed. Also, some comments about the presented scheme will be made.

2. Analytical model for half-space medium

The analytical model is a rigid circular plate on a half-space medium subjected to time harmonic loadings. The interaction tractions between plate and surrounding medium are shown in Fig. 1, and can be expressed in cylindrical coordinates in terms of Fourier components with respect to azimuth.

$$\begin{bmatrix} \overline{\tau_{rz}}(r,\theta) \\ \overline{\sigma_{zz}}(r,\theta) \\ \overline{\tau_{\theta z}}(r,\theta) \end{bmatrix} e^{i\omega t} = \sum_{n=0}^{1} \begin{bmatrix} \overline{\tau_{rz}}^{n}(r) \begin{Bmatrix} \cos(n\theta) \\ \sin(n\theta) \end{Bmatrix} \\ \overline{\sigma_{zz}}^{n}(r) \begin{Bmatrix} \cos(n\theta) \\ \sin(n\theta) \end{Bmatrix} \\ \overline{\tau_{\theta z}}^{n}(r) \begin{Bmatrix} -\sin(n\theta) \\ \cos(n\theta) \end{Bmatrix} \end{bmatrix} e^{i\omega t}; \quad 0 \leqslant r \leqslant a_0 \tag{1}$$

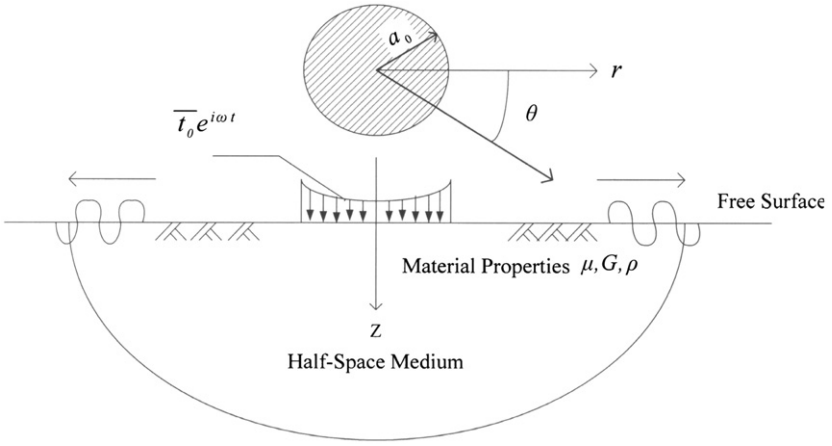

Fig. 1. Dynamic loading on half-space medium.

where the superscript n denotes the nth Fourier component in the series; in this rigid circular plate case, $n=0$ represents vertical (symmetric with respect to $\theta=0$) and torsional loadings (anti-symmetric), $n=1$ represents horizontal and rocking loadings (symmetric); $\omega=$ frequency; and a_0 is radius of circular plate. Since the time variation $e^{i\omega t}$ appears on both sides of the equation and can therefore be canceled, it is omitted hereinafter.

To solve 3D wave equations with prescribed tractions given by Eq. (1), some fundamental solutions in cylindrical coordinates can be exploited. Sezawa [15] developed a technique for separating the dilatational and rotational waves in the general equations of wave propagation, and used the technique of separation of variables to obtain general solution for nth Fourier component with respect to azimuth. After mathematical manipulation of the general solutions, one can express the displacement components at the surface $z=0$ in terms of the traction components on the surface for any nth Fourier component as follows:

$$\begin{bmatrix} u_r(r,0) \\ u_z(r,0) \\ u_\theta(r,0) \end{bmatrix} = \mathbf{J} \begin{bmatrix} -\nu' k_\beta^2/\Lambda & k(2\nu\nu' - 2k^2 + k_\beta^2)/\Lambda & 0 \\ k(2\nu\nu' - 2k^2 + k_\beta^2)/\Lambda & -\nu k_\beta^2/\Lambda & 0 \\ 0 & 0 & -1/G\nu' \end{bmatrix} \mathbf{J}^{-1} \begin{bmatrix} \tau_{rz}(r,0) \\ \sigma_{zz}(r,0) \\ \tau_{\theta z}(r,0) \end{bmatrix} \tag{2a}$$

or

$$\mathbf{u}_0 = \mathbf{J}\mathbf{Q}\mathbf{J}^{-1}\mathbf{t}_0 \tag{2b}$$

where

$$\mathbf{J} = \begin{bmatrix} J_n'(kr) & 0 & (n/r)J_n(kr) \\ 0 & kJ_n(kr) & 0 \\ (n/r)J_n(kr) & 0 & J_n'(kr) \end{bmatrix} \tag{2c}$$

$\Lambda = G[4k^2\nu\nu' - (2k^2 - k_\beta^2)^2]$; $\nu = \sqrt{k^2 - (\omega^2/c_p^2)}$; $\nu' = \sqrt{k^2 - (\omega^2/c_s^2)}$; $k_\beta = \omega/c_s$; c_P and c_s are compressional and shear wave velocities, respectively; G is shear modulus; k is wave number in the r-direction; $J_n(kr)$ is first kind of Bessel function of order n; and $J_n'(kr) = [\mathrm{d}J_n(kr)/\mathrm{d}r]$.

In order to simulate the arbitrary distributions of interaction tractions in r-direction , the distribution of tractions in r-direction of Eq. (1) is approximated by piecewise linear model. Assuming that the interval $(0,a_0)$ for Eq. (1) is divided into m subintervals with equal width $b=a_0/m$, one can express the variation for each

Fourier component in r-direction of Eq. (1) by the piecewise linear distribution as follows:

$$\overline{\tau_{rz}} = \sum_{j=1}^{m-1} h_j(r)p_j + h_0(r)p_0 + h_m(r)p_m = \mathbf{h}^T\mathbf{p}$$
$$\overline{\sigma_{zz}} = \sum_{j=1}^{m-1} h_j(r)q_j + h_0(r)q_0 + h_m(r)q_m = \mathbf{h}^T\mathbf{q}$$
$$\overline{\tau_{\theta z}} = \sum_{j=1}^{m-1} h_j(r)s_j + h_0(r)s_0 + h_m(r)s_m = \mathbf{h}^T\mathbf{s} \tag{3}$$

where

$$h_j(r) = \begin{cases} 1 + \dfrac{r-jb}{b} & \text{if } (j-1)b \leqslant r \leqslant jb \text{ and } 1 \leqslant j \leqslant m \\ 1 - \dfrac{r-jb}{b} & \text{if } jb \leqslant r \leqslant (j+1)b \text{ and } 0 \leqslant j \leqslant m-1 \\ 0 & \text{otherwise} \end{cases} \tag{3a}$$

and p_j, q_j and s_j are the traction intensities at node j for $\overline{\tau_{rz}}$, $\overline{\sigma_{zz}}$ and $\overline{\tau_{\theta z}}$, respectively. Liou [13] has developed a technique to decompose the tractions in Eqs. (3) as follows:

$$\begin{aligned} \begin{bmatrix} \overline{\tau_{rz}}(r) \\ \overline{\sigma_{zz}}(r) \\ \overline{\tau_{\theta z}}(r) \end{bmatrix} &= \begin{bmatrix} 1 \\ 0 \\ -1 \end{bmatrix} \left(\frac{\overline{\tau_{rz}}(r) - \overline{\tau_{\theta z}}(r)}{2} \right) + \begin{bmatrix} 0 \\ 1 \\ 0 \end{bmatrix} \overline{\sigma_{zz}}(r) + \begin{bmatrix} 1 \\ 0 \\ 1 \end{bmatrix} \left(\frac{\overline{\tau_{rz}}(r) + \overline{\tau_{\theta z}}(r)}{2} \right) \\ &= \begin{bmatrix} 1 \\ 0 \\ -1 \end{bmatrix} \frac{1}{2}[\mathbf{h}^T, 0, -\mathbf{h}^T] \begin{bmatrix} \mathbf{p} \\ 0 \\ \mathbf{s} \end{bmatrix} + \begin{bmatrix} 0 \\ 1 \\ 0 \end{bmatrix} [0, \mathbf{h}^T, 0] \begin{bmatrix} 0 \\ \boldsymbol{q} \\ 0 \end{bmatrix} + \begin{bmatrix} 1 \\ 0 \\ 1 \end{bmatrix} \frac{1}{2}[\mathbf{h}^T, 0, \mathbf{h}^T] \begin{bmatrix} \mathbf{p} \\ 0 \\ \mathbf{s} \end{bmatrix} \\ &= \int_0^\infty \begin{bmatrix} 1 \\ 0 \\ -1 \end{bmatrix} kJ_{n+1}(kr)[\mathbf{D}_{n+1}^T, 0, -\mathbf{D}_{n+1}^T] \begin{bmatrix} \mathbf{p} \\ 0 \\ \mathbf{s} \end{bmatrix} \mathrm{d}k \\ &\quad + \int_0^\infty \begin{bmatrix} 0 \\ 1 \\ 0 \end{bmatrix} kJ_n(kr)[0, \mathbf{D}_n, 0] \begin{bmatrix} 0 \\ \mathbf{q} \\ 0 \end{bmatrix} \mathrm{d}k + \int_0^\infty \begin{bmatrix} 1 \\ 0 \\ 1 \end{bmatrix} kJ_{n-1}(kr)[\mathbf{D}_{n-1}, 0, \mathbf{D}_{n-1}] \begin{bmatrix} \mathbf{p} \\ 0 \\ \mathbf{s} \end{bmatrix} \mathrm{d}k \end{aligned} \tag{4}$$

where

$$\mathbf{D}_{n+1}^T = \int_0^{a_0} \frac{r}{2} J_{n+1}(kr)\mathbf{h}^T \,\mathrm{d}r$$
$$\mathbf{D}_n^T = \int_0^{a_0} rJ_n(kr)\mathbf{h}^T \,\mathrm{d}r \tag{4a}$$

and

$$\mathbf{D}_{n-1}^T = \int_0^{a_0} \frac{r}{2} J_{n-1}(kr)\mathbf{h}^T \,\mathrm{d}r$$

The integrals on the right hand side of third equal sign in Eq. (4) and integrals in Eqs. (4a) are Hankel transform pairs, respectively. One should also notice that the vectors $(1,0,-1)^T$, $(0,1,0)^T$ and $(1,0,1)^T$ are orthogonal eigenvectors corresponding to eigenvalues $-kJ_{n+1}(kr)$, $kJ_n(kr)$ and $kJ_{n-1}(kr)$ of the Bessel function

matrix **J** in Eq. (2c). Therefore, Eq. (4) can be replaced with the following equation.

$$\begin{bmatrix} \overline{\tau_{rz}} \\ \overline{\sigma_{zz}} \\ \overline{\tau_{\theta z}} \end{bmatrix} = \int_0^\infty \mathbf{J} \begin{bmatrix} -\mathbf{D}_{n+1}^T + \mathbf{D}_{n-1}^T & 0 & \mathbf{D}_{n+1}^T + \mathbf{D}_{n-1}^T \\ 0 & \mathbf{D}_n^T & 0 \\ \mathbf{D}_{n+1}^T + \mathbf{D}_{n-1}^T & 0 & -\mathbf{D}_{n+1}^T + \mathbf{D}_{n-1}^T \end{bmatrix} \begin{Bmatrix} \mathbf{q} \\ \mathbf{p} \\ \mathbf{s} \end{Bmatrix} \mathrm{d}k$$
$$= \int_0^\infty \mathbf{JDP}\,\mathrm{d}k \tag{5}$$

Using $\mathbf{t}_0 = -\overline{\mathbf{t}_0}$ and substituting $\mathbf{t}_0 = -\mathbf{JDP}\,\mathrm{d}k$ from Eq. (5) into Eq. (2b), the following equation can be obtained by integrating the resulting expression from 0 to ∞.

$$\mathbf{u}_0 = -\int_0^\infty \mathbf{JQDP}\,\mathrm{d}k \tag{6}$$

Eq. (6) can be employed to calculate the vibration at any specific location on half-space medium ($z = 0$), if the intensity vector **P** described in Eqs. (3) is known. For the vibration at arbitrary location in half-space medium ($z \neq 0$), the formulations above should be re-derived to include the vertical variations ($e^{-v'z}$ and e^{-vz}) of vibrations. But the paper will focus on calculating the vibrations on half-space medium for simplicity.

For the cases of rigid circular foundation excited by vertical and horizontal forces, and torsional and rocking (or pitching) moments, the impedance matrix has to be found first. As stated by Liou et al. [14], to find the impedance matrix, finite element model for displacement field of foundation itself is assumed and variational principle (principle of virtual work) and reciprocal theorem are employed. Then, the intensity vector **P** in Eqs. (3) and (6) can be obtained for all the excitation forces and moments in the process of finding impedance matrix.

For the cases of rigid circular foundation, the displacement fields in the foundation can be assumed as follows: $u_\theta(r,\theta) = v_1 r$ ($n = 0$ of anti-symmetric mode) for excitation of torsional moment, $u_z(r,\theta) = v_2$ ($n = 0$ of symmetric mode) for excitation of vertical force, and $u_z(r,\theta) = v_3 r\cos\theta$, $u_r(r,\theta) = v_4\cos\theta$ and $u_\theta(r,\theta) = -v_4\sin\theta$ ($n = 1$ of symmetric mode) for excitations of rocking moment and horizontal force. In the expressions, v_1 is the unknown generalized displacement at center of foundation for torsional excitation, v_2 is for vertical excitation, and v_3 and v_4 are, respectively, for rocking and horizontal excitations which are coupled.

With these displacement fields, the impedance matrix and interaction traction in Eq. (3) can therefore be calculated for a rigid circular foundation subjected to harmonic loadings.

3. Numerical investigations

In the semi-infinite integration of Eq. (6), singular point may exist, provided there is no damping assumed for half-space medium. This is because $\Lambda = 0$ in matrix **Q** in Eq. (2a) when wave number k is equal to Rayleigh wave number. Although technique such as residue theorem may be used to calculate the integration around the singular point, material damping is introduced in half-space medium in order to comply with more realistic situation of medium, and hysteretic type of damping is chosen. This means shear modulus G in Eqs. (2a), (2b) and (2c) is complex and can be expressed as $G = \overline{G}(1 + 2\xi i)$ in which ξ is damping ratio. Therefore, numerical integration scheme can be directly employed. Furthermore, using the following three statements, the integrand in the semi-infinite integral of Eq. (6) can be easily shown to be proportional to $1/k^2$ as $k \to \infty$:

(1) The elements of matrix **J** are proportional to $k^{0.5}$ as $k \to \infty$.
(2) The elements of matrix **Q** decay with $1/k$ as $k \to \infty$, since $v \doteq v' \doteq k$ as $k \to \infty$.
(3) Using the identities of $\int r^2 J_n(kr)\,\mathrm{d}r = -(r^2/k)J_{n+1}(kr) + ((n+1)/k)\int rJ_{n-1}(kr)\,\mathrm{d}r$ and $\int rJ_n(kr)\,\mathrm{d}r = -(r/k)J_{n-1}(kr) + (n/k)\int J_{n-1}(kr)\,\mathrm{d}r$, and $J_n(kr) \propto 1/k^{0.5}$ as $k \to \infty$, it is concluded that the elements of

matrix **D** in Eqs. (4), (4a), (5) and (6) decay with $1/k^{1.5}$. Therefore, it is appropriate to replace the infinite integration limit with a finite number without losing accuracy.

To perform the integrations in Eq. (6) and **D** matrix in Eqs. (4a), method of Gaussian Quadrature is employed. In order to simplify the following discussion of the integrations, the radius of foundation a_0 in Eqs. (4a), distance r and wave number k in Eqs. (4a) and (6) have been nondimensionalized by the shear wave length λ of frequency 1 Hz. The wave length $\lambda = Re(c_s)/1\,\mathrm{s}$, in which $Re(c_s)$ is real part of shear wave velocity c_s. Complex c_s is due to complex shear modulus G. To exploit Gaussian Quadrature integration method, the sizes of integration subinterval with corresponding number of integration points has to be chosen first. To do the integration of **D** matrix in Eqs. (4a), the subinterval Δr with 4 Gaussian integration points is chosen by the formula $\Delta rk/\pi \leqslant 1$. To do the integration in Eq. (6), the subinterval Δk with 5 Gaussian points is chosen by the formula $\Delta k \cdot r/\pi \leqslant 1$ for $k > 1.3k_R$ in which k_R is Rayleigh wave number and r is the distance of the location where vibration is calculated. For $k \leqslant 1.3k_R$, the subinterval Δk with 5 Gaussian points is calculated by $\Delta k \cdot r/\pi \leqslant 0.1$, since the variation of integrand for k close to compressional wave number, shear wave number and Rayleigh wave number is much more dramatic. Using the above integration criteria, the precision of the semi-infinite integration of Eq. (6) with integration upper limit ∞ replaced by arbitrary k_u can be maintained up to 6 significant figures for all the numerical results presented in the paper.

After some convergence study, the followings can also be concluded: (1) $m = 20$ for the number of subinterval in Eqs. (3) is enough to accurately describe the distribution of interaction tractions between plate and half-space medium; and (2) In general, the integration upper limit k_u for Eq. (6) must be larger as the nondimensional distance from plate center is farther, or excitation frequency is higher.

Although greater hysteretic damping in half-space medium will generally leads to a larger upper integration limit k_u in order to maintain same accuracy of vibration amplitude by Eq. (6), the increment of k_u is not significant while compared with the other two factors which are distance and frequency. To investigate how large k_u is needed for different distances from foundation center and excitation frequencies, k_u like r, k and a_0 has also been nondimensionalized with the shear wave length λ of frequency 1 Hz. If one wants to obtain the vibration amplitude with less than 1 percent discrepancy, k_u to replace ∞ in the integration of Eq. (6) can be selected for some cases as follows:

(1) When nondimensional frequency $\omega a_0 \cdot 1\,\mathrm{s}/2\pi = 1.0$, nondimensional k_u should be greater than 650, 1000, 2100, 6200, 15000 and 30000 for calculating the vibration amplitude at nondimensional distance $\omega r \cdot 1\,\mathrm{s}/2\pi = 10,20,40,60,80$ and 100, respectively.
(2) k_u should be greater than 1200 for calculating the vibration amplitude at $\omega r \cdot 1\,\mathrm{s}/2\pi = 10$ with $\omega a_0 \cdot 1\,\mathrm{s}/2\pi = 0.00005$ and k_u should be greater than 850 for calculating the vibration amplitude at $\omega r \cdot 1\,\mathrm{s}/2\pi = 10$ with $\omega a_0 \cdot 1\,\mathrm{s}/2\pi = 0.1$.

From the above numerical test, one can conclude that $k_u = 1200$, for nondimensional frequency $\omega a_0 \cdot 1\,\mathrm{s}/2\pi$ between 0.00005 and 1.0 and nondimensional distance $\omega r \cdot 1\,\mathrm{s}/2\pi$ up to 10, is necessary for calculating vibration amplitude by Eq. (6) with 1 percent discrepancy. One should also notice that $\omega r \cdot 1\,\mathrm{s}/2\pi = 10$ is equivalent to 10 times of shear wave length. The discrepancy is defined by the percentage of the difference between two numerical results, respectively, with integration upper limits k_u and $2k_u$ to the result with k_u. Therefore, one can conclude that the presented scheme is numerically convergent and the numerical integration is straight forward without any difficulty.

Also, one can observe that larger k_u is necessary for larger nondimensional distance $\omega r \cdot 1\,\mathrm{s}/2\pi$ and larger k_u is also needed for larger nondimensional frequency $\omega a_0 \cdot 1\,\mathrm{s}/2\pi$ if r is fixed; e.g. r from $\omega r \cdot 1\,\mathrm{s}/2\pi = 100$ with nondimensional frequency $\omega a_0 \cdot 1\,\mathrm{s}/2\pi = 1.0$, in which $k_u = 30000$ is needed as stated above in (1), is the same as r from $\omega r \cdot 1\,\mathrm{s}/2\pi = 10$ with nondimensional frequency $\omega a_0 \cdot 1\,\mathrm{s}/2\pi = 0.1$, in which $k_u = 850$ is needed as stated above in (2).

Since the total system is linear, all the quantities can be nondimensionalized. As shown in Ref. [14], the torsional, vertical, horizontal, coupling and rocking impedance functions are nondimensionalized, respectively, as follows: I_{TT}/Ga_0^3, I_{vv}/Ga_0, I_{HH}/Ga_0, I_{HR}/Ga_0^2, and I_{RR}/Ga_0^3. Therefore, the excitation forces are normalized in the similar way. The vertical and horizontal excitation forces are nondimensionalized in the

forms of $F_V/Ga_0\lambda$ and $F_H/Ga_0\lambda$, respectively, in which λ is the shear wave length of frequency 1 Hz. The torsional and rocking excitation moments are normalized in the forms of $M_T/Ga_0^3\lambda$ and $M_R/Ga_0^3\lambda$, respectively. The reason to manipulate the quantities in this way is to made the following numerical results of u_r, u_z and u_θ have been nondimensionalized by λ. The numerical results shown in the following table and figures are produced by unit harmonic excitation forces. This means $F_V = Ga_0\lambda$, $F_H = Ga_0\lambda$, $M_T/Ga_0^3\lambda$ or $M_R/Ga_0^3\lambda = 1$.

In the numerical results, the hysteretic damping ratios $\xi = 0.0001$, 0.001, 0.01, 0.02, and 0.03 are selected for half-space medium and the Poisson ratios are assumed to be 0.0, 0.25, 0.33 and 0.45. The reason to select the case of very low damping ($\xi = 0.0001$) is to check and approximate the behavior of vibration in the medium without material damping. In order to validate the presented scheme, the case for small nondimensional frequency $\omega a_0 \cdot 1\,\mathrm{s}/2\pi = 0.00005$ and $\xi = 0.0001$ is employed to simulate the point source problem and the numerical results are compared with that for the point source case by Apsel and Ruco [13]. Table 1 shows the comparison. Comparing with Apsel and Ruco's results, one should notice that the force units are different for both schemes . However, the total system of half-space medium for both cases are linearly elastic. The excitation forces can be scaled to the same level for both schemes. This can be done by scaling one component of the present results to the same value by point source excitation. And then all the other components of the presented results are multiplied with the scale factor. In Table 1, real part of $r_0/4\pi u_{r1}$ with $r_0 = 5.5$ (in the last row of the table) by the presented method is scaled to 0.044 which is Apsel and Ruco results. The 0.44 by both the presented and Apsel and Ruco methods are indicated bold in Table 1. In the table, the first two columns are Apsel and Ruco's results, the last two columns are the present results, the upper half is for vertical

Table 1
Comparison with result of point source case.

$r_0 = \omega r \cdot 1\,\mathrm{s}$	Apsel and Ruco's results with 0.01% damping ($\times 10^{-3}$)				Present results with 0.01% damping and nondimensional frequency $\omega \cdot a_0 \cdot 1\,\mathrm{s}/2\pi = 0.00005$ ($\times 10^{-3}$)			
	$\frac{r_0}{4\pi}u_{r0}(r_0,0)$		$\frac{r_0}{4\pi}u_{z0}(r_0,0)$		$\frac{r_0}{4\pi}u_{r0}(r_0,0)$		$\frac{r_0}{4\pi}u_{z0}(r_0,0)$	
0.5	−32	7	88	−61	−32.2	7.16	87.2	−61.5
1.0	−33	25	37	−102	−33.1	25.5	36.9	−102
1.5	−21	46	−28	−108	−20.6	46.8	−28.3	−108
2.0	6	60	−87	−77	6.14	60.6	−86.9	−76.4
2.5	41	57	−120	−17	41.1	58.0	−119	−16.3
3.0	73	35	−114	53	73.5	35.1	−113	53.1
3.5	92	−6	−71	109	91.8	−5.21	−69.2	109
4.0	87	−54	−2	134	86.8	−53.5	−0.13	134
4.5	57	−96	72	117	56.2	−96.3	73.0	117
5.0	6	−120	127	63	5.12	−120	127	62.5
5.5	-54	−115	145	−13	−54.4	−115	144	−14.2
	$\frac{r_0}{4\pi}u_{r1}(r_0,0)$		$\frac{r_0}{4\pi}u_{\theta 1}(r_0,0)$		$\frac{r_0}{4\pi}u_{r1}(r_0,0)$		$\frac{r_0}{4\pi}u_{\theta 1}(r_0,0)$	
0.5	146	−58	−90	58	145	−58.3	−90.0	57.4
1.0	112	−105	−46	99	110	−105	−46.4	98.7
1.5	62	−133	13	112	61.3	−132	13.0	112
2.0	9	−137	73	93	8.57	−136	72.2	92.7
2.5	−37	−120	115	45	−36.9	−119	114	45.0
3.0	−68	−90	128	−20	−67.4	−88.4	127	−19.2
3.5	−81	−55	107	−84	−80.0	−53.3	106	−83.6
4.0	−78	−24	56	−131	−77.0	−23.0	55.6	−131
4.5	−66	−4	−15	−149	−64.8	−3.45	−14.3	−147
5.0	−52	4	−87	−129	−51.5	4.28	−85.9	−128
5.5	**−44**	3	−142	−77	**−44**	3.48	−141	−76.1

excitation ($n = 0$), and the lower half is for horizontal excitation ($n = 1$). From the table, one can see that both results fairly agree to each other.

Figs. 2–6 show the results of vibration amplitudes along the nondimensional distance from center of circular plate. Figs. 2–4 show the results for the cases of nondimensional frequencies $\overline{\omega} = \omega a_0 \cdot 1/2\pi = 0.00005$ and 1.0 with Poisson ratio $\mu = 0.33$. The small nondimensional frequency can be used to approximate point source excitation problem and nondimensional frequency 1.0 can be used to observe the behavior for the case of high frequency. Fig. 2 shows the vibration amplitude of u_θ component due to unit normalized torsional moment excitation. From the figure, one can see that for $\omega r \cdot 1\, s/2\pi - \omega a_0 \cdot 1/2\pi \leqslant 0.5$ the attenuation of vibration is mainly caused by spatial dilution and for $\omega r \cdot 1/2\pi - \omega a_0 \cdot 1/2\pi \geqslant 0.5$ material damping is getting more significant for attenuation of vibration. Also, the vibration decays along the distance smoothly. Figs. 3 and 4 show the vibration amplitudes of u_r and u_z, respectively, due to unit nondimensional vertical force. Looking at these two figures, one can observe that the vibration attenuates over the distance only from marco view of point, and the amplitudes of vibration along the distance may fluctuate. The fluctuation becomes more dramatic as damping and frequency getting higher and the period of the fluctuation over the nondimensional distance is about 1.80∼1.90 in the figures. Trying to interpret this phenomenon, one can refer to Eqs. (6) and (2a). The $1/\Lambda$ in **Q** matrix of Eqs. (6) or (2a) will be getting huge as k is close to Rayleigh wave number. Therefore, the contribution of the wave number components in the neighborhood of Rayleigh wave number is very important in the integration of Eq. (6). Also, the numerical values of elements in matrix **Q** vary more

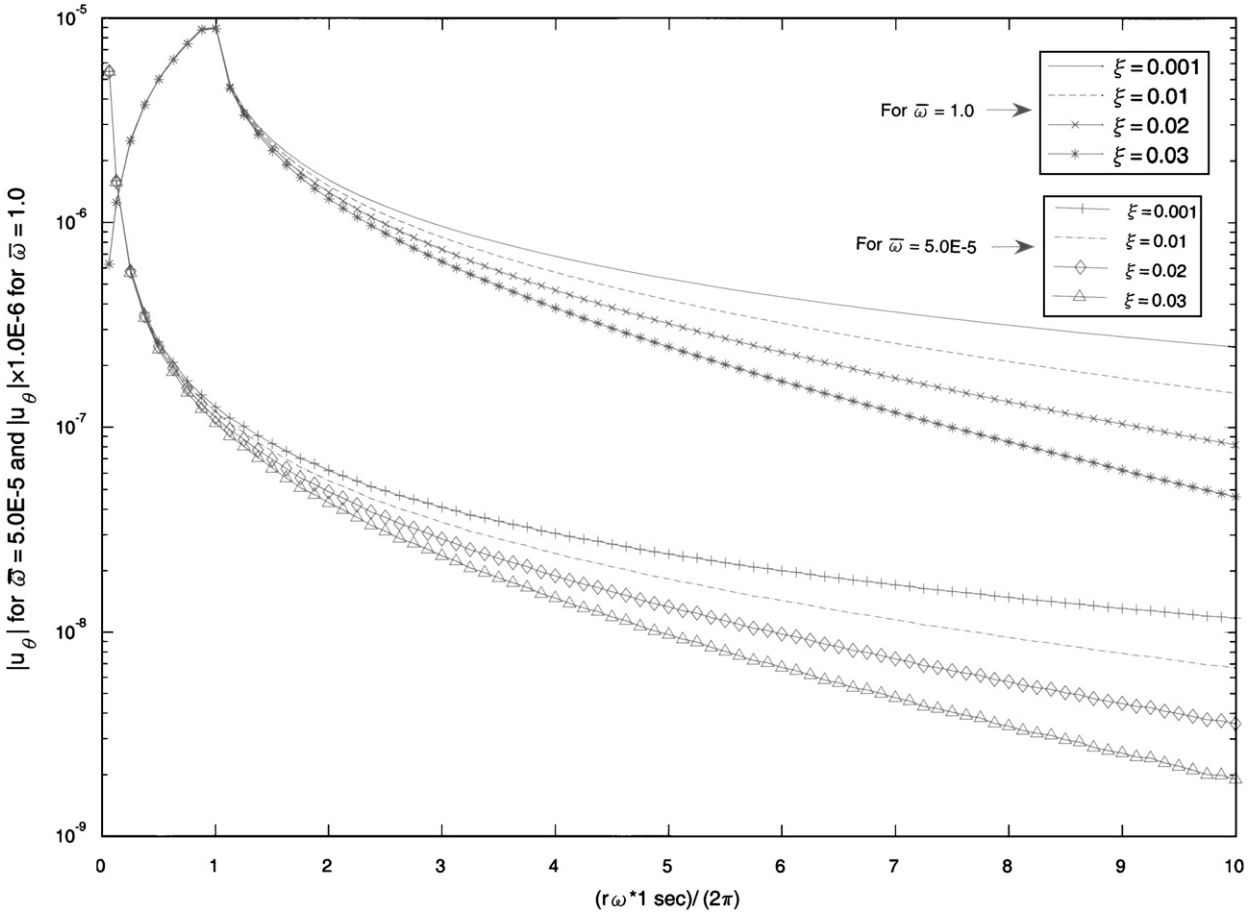

Fig. 2. Vibration amplitude of u_θ due to unit normalized torsional excitation.

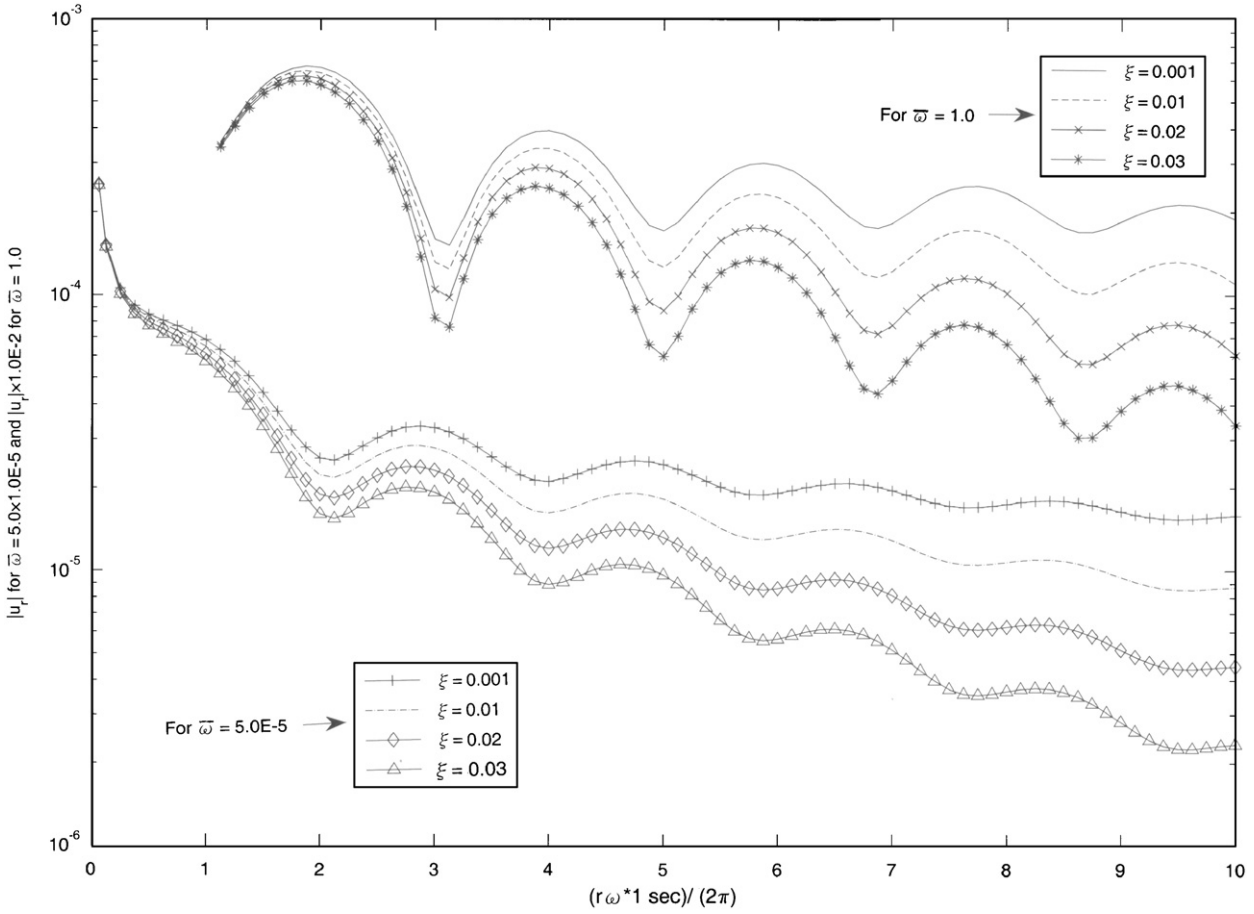

Fig. 3. Vibration amplitude of u_r due to unit nondimensional vertical excitation.

drastically as wave number k approaching compressional and shear wave numbers. This indicates that the wave number components in the neighborhoods of compressional and shear wave number are important too. The fluctuation could be caused by the interaction of these properties. In Fig. 3, one should notice that some curves start from $\omega r \cdot 1\,\mathrm{s}/2\pi = 1$. This is due to welded condition has been assumed at interface of foundation and half-space medium. This assumption leads to $u_\theta = 0$ under the foundation. For the cases of foundation subjected to harmonic horizontal force and rocking harmonic moment, the similar fluctuation phenomenon can be observed in the numerical results which are not shown in the paper. One should also notice that the phenomenon mentioned above does not occur in the torsional case (Fig. 2). For torsional excitation, only *SH* wave is generated.

The above mentioned interesting phenomenon leads to the curiosity of finding the average energy flux intensity at $z = 0$. The average flux intensity is defined by the formula as follows:

$$\overline{E} = \rho\omega^2 \frac{\omega}{2\pi}\frac{1}{2\pi}\int_0^{\omega/2\pi}\int_0^{2\pi}(|u_r|^2 + |u_z|^2 + |u_\theta|^2)\begin{pmatrix}\sin^2 n\theta \\ \cos^2 n\theta\end{pmatrix} \mathrm{d}\theta\, \mathrm{e}^{2\mathrm{i}\omega t}\,\mathrm{d}t \tag{7}$$

where ρ is mass density. The flux intensity in Eq. (7) is the averaging over time period $2\pi/\omega$ and circle length $2\pi r$. Eq. (7) is easy to be integrated. The $\overline{E}$ can be normalized to become the following equation without losing

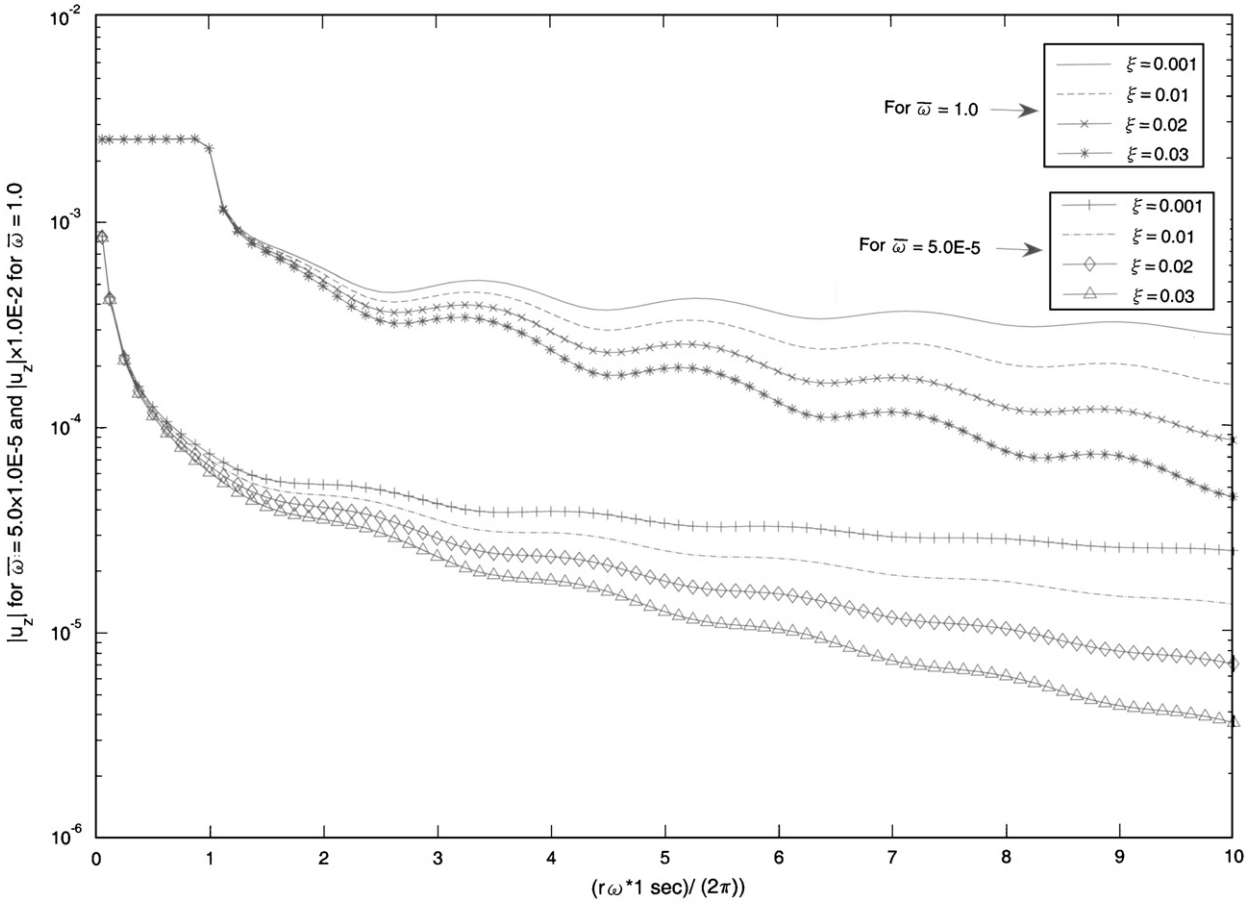

Fig. 4. Vibration amplitude of u_z due to unit nondimensional vertical excitation.

the meaning of average energy flux intensity.

$$E = |u_r|^2 + |u_z|^2 + |u_\theta|^2 \tag{8}$$

Now, one can employ Eq. (8) to calculate E for different distances from the center of foundation. The results are shown in Fig. 5. From the figure, one observes that the fluctuation is smaller. It is also believed that the curve for average energy flux intensity will be smoother for greater z, since Rayleigh wave is confined in the depth near free surface.

The fluctuation phenomenon is also investigated by changing Poisson ratio. Fig. 6 shows the results for the component of u_r induced by horizontal vibration of foundation for the cases with different Poisson ratios which are 0.0, 0.25, 0.33 and 0.45.

In the figure, nondimensional frequency $\omega a_0 \cdot 1\,\mathrm{s}/2\pi = 0.1$ and damping ratio $\xi = 0.02$ are assigned. From the figure one can observe the following two phenomena: (1) The period of fluctuation is getting longer as Poisson ratio becomes smaller. For example, the periods are about 2.3–2.4, 2.0–2.1, 1.8–1.9 and 1.6–1.7 along nondimensional distance $\omega r \cdot 1\,\mathrm{s}/2\pi$ for Poisson ratios $\mu = 0.0$, 0.25, 0.33 and 0.45, respectively; (2) At the first few cycle of fluctuation, the fluctuation is more drastic for higher Poisson ratio. Also, from this investigation,

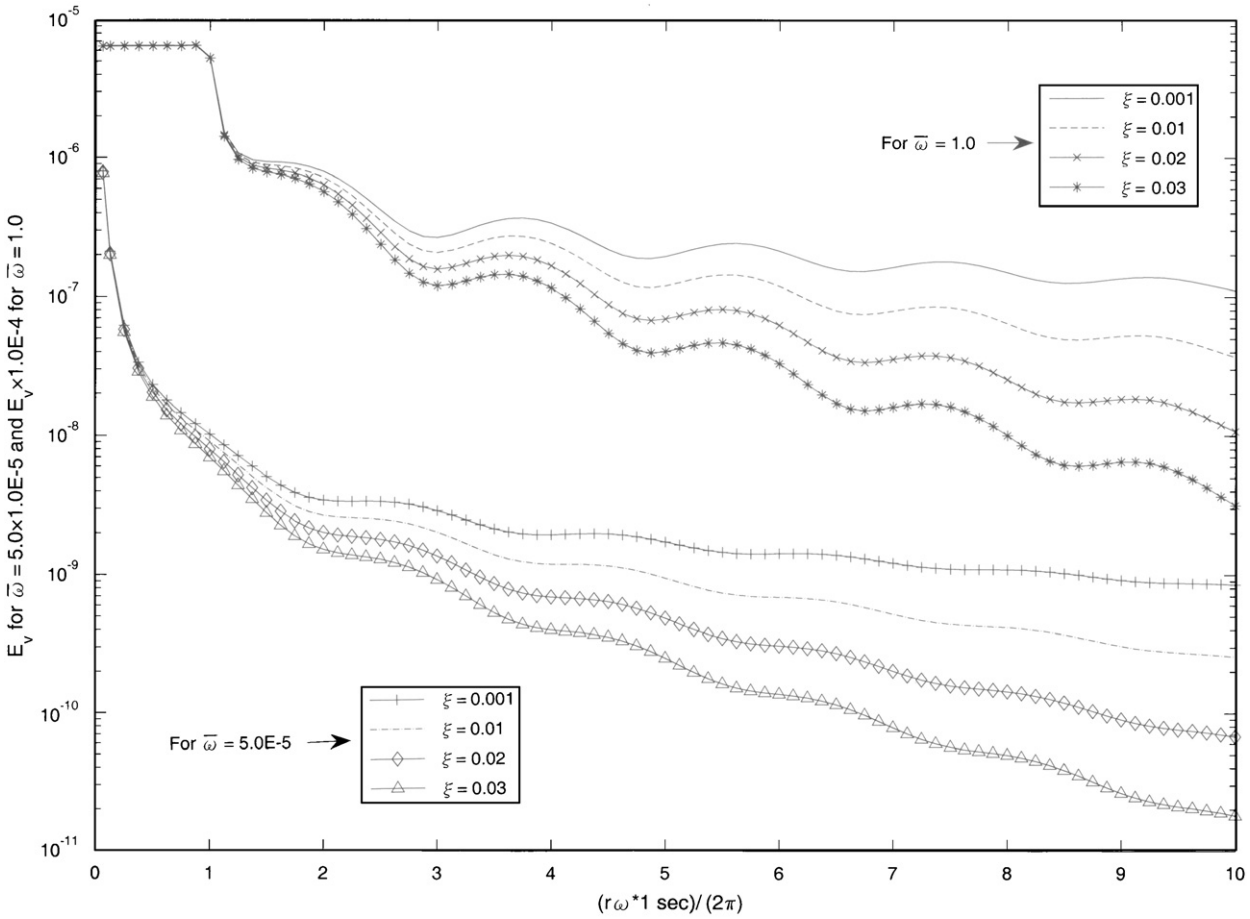

Fig. 5. Average energy flux intensity due to unit nondimensional vertical excitation.

the period of the fluctuation is mainly corresponding to the change of Poisson ratio and less influenced by changes of frequency and damping.

4. Concluding remarks

The presented scheme can be combined with finite element model of superstructure to directly calculate the vibration on half-space medium due to vibration of superstructure, if one assumes the foundation on the half-space is rigid and circular. Although the vibration is calculated at surface ($z = 0$) by the presented scheme, it is possible to extend the scheme to calculate the vibration at depth ($z \neq 0$) and the vibration induced by vibration of foundation with arbitrary shapes. For the cases of the foundation with arbitrary shapes, more Fourier components in Eq. (1) must be simultaneously incorporated in the calculation.

One should notice that the fluctuation phenomenon shown in the numerical results is for single Fourier component ($n = 0$ or $n = 1$) with single frequency between ($\omega a_0 \cdot 1\,\text{s}/2\pi = 0.00005$–$1.0$). For the cases with combination of many frequency components (e.g. time history excitation) and combination of many Fourier components in Eq. (1) (e.g. foundation with arbitrary shape), the fluctuation could be flattened.

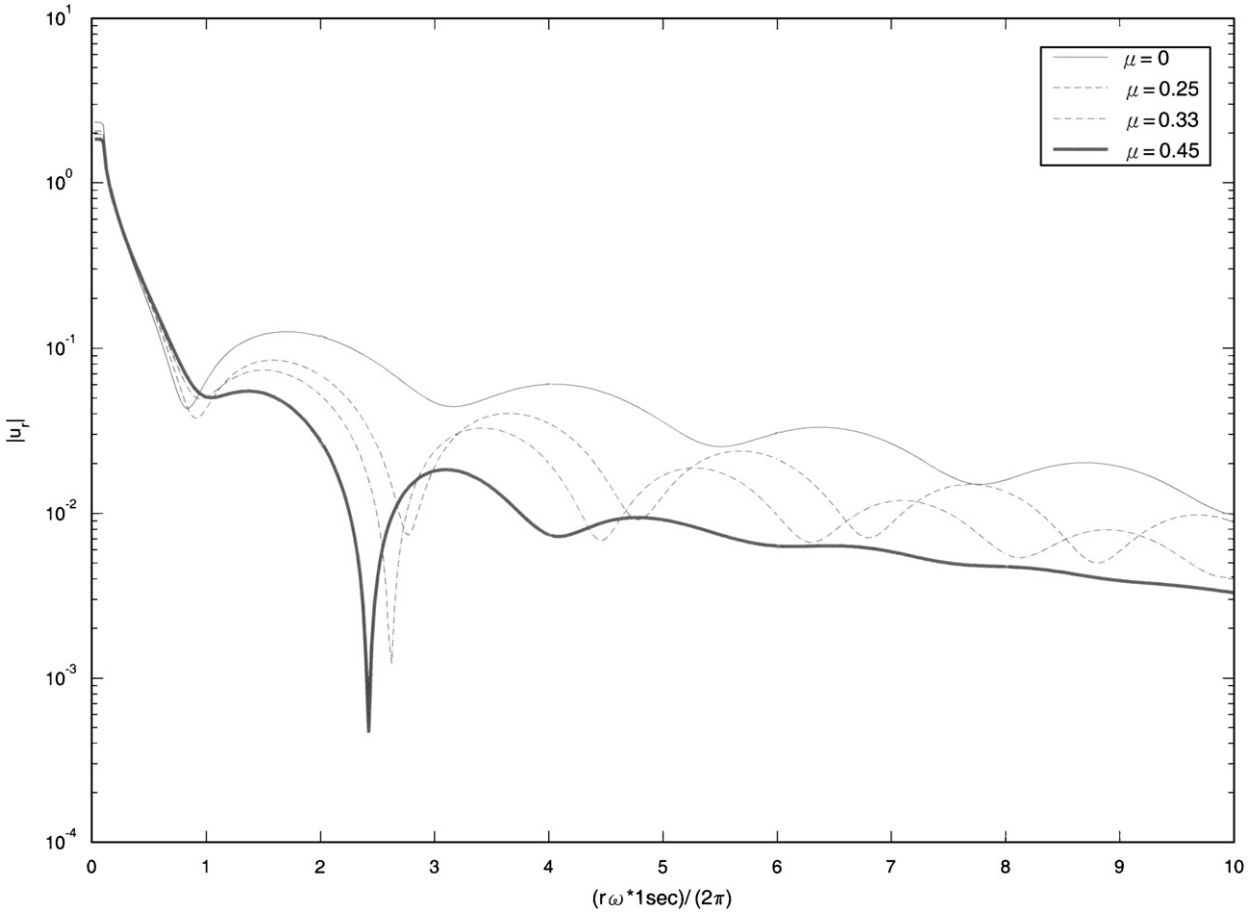

Fig. 6. Vibration amplitude of u_r due to unit nondimensional horizontal excitation.

The integrations of the presented scheme is simply straight forward and self-proved convergence. Therefore, in terms of computational cost and numerical precision, the presented method is better than finite element and boundary element based methods for the problems which can be dealt with by the presented method.

Acknowledgments

The financial support of this research is partly provided by National Science Council of Taiwan through Contract no. 96-2221-E-009-082. During preparation of the manuscript, Professor Y.J. Lee of National Ilan University has given some valuable suggestions.

References

[1] C.G. Gordon, T.L. Dresner, Methods of developing vibration and acoustic noise specifications for microelectronics process tools, *Vibration Monitoring and Control SPIE Proceedings*, Vol. 2264, July 1994.

[2] X. Sheng, C.J.C. Jones, M. Petyt, Ground vibration generated by a load moving along a railway track, *Journal of Sound and Vibration* 228 (1) (1999) 129–156.

[3] V.V. Krylov, Vibrational impact of high-speed trains. I: effect of track dynamics, *Journal of the Acoustical Society of America* 100 (5) (1996) 3121–3134.

[4] A.M. Kaynic, C. Madshus, P. Zackrisson, Ground vibration from high-speed train: prediction and countermeasure, *Journal of Geotechnical and Geoenvironmental Engineering* 126 (6) (2000) 0531–0573.

[5] H. Takemiya, X. Bian, Substructure simulation of inhomogeneous track and layered ground dynamic interaction under train passage, *Journal of Engineering Mechanics* 131 (7) (2005) 699–711.
[6] H. Takemiya, Simulation of track-ground vibrations due to high-speed train: the case of X-2000 at Ledsgard, *Journal of Sound Vibration* 261 (2003) 503–526.
[7] S. Ahmad, T.M. Al-Hussaini, Simplified design for vibration screening by open and in-filled trenches, *Journal of Geoenvironmental Engineering, ASCE* 117 (1) (1991) 67–88.
[8] B. Dasgupta, D.E. Beskos, I.G. Vardoulakis, Vibration isolation using open or filled trenches, part 2, 3D homogenous soil, *Computational Mechanics* (1990) 129–142.
[9] H. Takemiya, Field vibration mitigation by honeycomb WIB for pile foundations of a high-speed train viaduct, *Soil Dynamics and Earthquake Engineering* 24 (2004) 69–87.
[10] G.F. Miller, H. Pursey, On the partition of energy between elastic waves in a semi-infinite solid, *The Royal Society of London Series A, Mathematical and Physical Sciences* 233 (6) (1955) 55–69.
[11] R.J. Apsel, J.E. Luco, On the Green's functions for a layered half-space, part II, *Bulletin of Seismological Society of America* 73 (4) (1983) 931–951.
[12] R.D. Woods, P.J. Larry, Energy-attenuation relationships from construction vibrations, *Proceedings of Vibration Problems in Geotechnical Engineering Convention*, Detroit, Michigan, 1985, pp. 229–246.
[13] G.-S. Liou, Analytical solution for soil–structure interaction in layered media, *Journal of Earthquake Engineering and Structural Dynamics* 18 (5) (1989) 667–686.
[14] G.-S. Liou, G.C. Lee, R. Ketter, Analytic solution for dynamic loading on half-space medium, *Journal of Engineering Mechanics ASCE* 117 (7) (1991) 1485–1493.
[15] K. Sezawa, Further studies on Rayleigh waves having some azimuthal distribution, *Bulletin of Earthquake Research Institute, University of Tokyo, Japan* 6 (1929) 1–18.